Chinese Chemical Letters 35 (2024) 109256

Contents lists available at ScienceDirect

Chinese Chemical Letters

journal homepage: www.elsevier.com/locate/cclet

Evolution of hollow nanosphere to microtube in the self-assembly of chiral dansyl derivatives and inversed circularly polarized luminescence

Sifan Du[a,b], Yuan Wang[b], Fulin Wang[b], Tianyu Wang[a,*], Li Zhang[b,*], Minghua Liu[b,*]

[a] Beijing Key Laboratory for Science and Application of Functional Molecular and Crystalline Materials, Department of Chemistry and Chemical Engineering, School of Chemistry and Biological Engineering, University of Science and Technology Beijing, Beijing 100083, China
[b] National Laboratory for Molecular Science (BNLMS), CAS Key Laboratory of Colloid, Interface and Chemical Thermodynamics, Institute of Chemistry, Chinese Academy of Sciences, Beijing 100190, China

ARTICLE INFO

Article history:
Received 11 July 2023
Revised 16 October 2023
Accepted 27 October 2023
Available online 30 October 2023

Keywords:
CPL inversion
Hollow structure
Self-assembly
Dansyl
Chirality transfer

ABSTRACT

Here, we designed asymmetric (mDS) and symmetrical (dDS) chiral V-shaped molecules by linking one or two dansyl groups to *trans*-1,2-cyclohexane diamine and investigated the solvent-regulated structural transformation and inversed circularly polarized luminescence (CPL) in the self-assemblies. Upon increasing water volume fraction (f_w) in the mixed solvent of water/acetonitrile, asymmetric mDS self-assembled into hollow nanospheres and microtubes, while solid nanospheres and solid microplates were corresponding to symmetric dDS. During this transformation process, the emission of mDS and dDS was changed from yellow-green to blue and cyan color, which was ascribed to twisted intramolecular charge transfer (TICT) and locally excited (LE) fluorescence of V-shaped DS molecules. The conformation of *N,N*-dimethyl groups with respect to naphthalene ring also led to the transformation of structures. These tubular and platelike structures had stronger and reversed CPL signals in comparison with spheroidal structures. The chiral information of DS assembly could be effective transferred to achiral Nile red *via* co-assembly strategy, which endowed Nile red exhibiting inversed induced CPL signal regulated by water fraction. This work provides a method for achieving a variety of self-assembled structures with adjustable chiroptical properties.

The hollow structures are common structures in nature, such as stems of bamboo, reeds, blood vessels and bones. These hollow structures are crucial to the survival of the living creatures due to their excellent material transport capacity, high mechanical strength, and light weight. Inspired by nature, researchers have prepared many kinds of hollow structure [1–15] including hollow spheres and tubular structures and developed their application in the field of catalyst carriers [16–18], drug capsules [19,20], pollutant removers [21]. Fabrication of hollow structures from organic molecules would be benefit from the view of improving compatibility with the living creatures. Self-assembly of organic small molecules is supposed to not only be a convenient method to acquire hollow structures, but the diversity of assembled structures [22–24] could be easily adjusted by the assembling condition or external conditions. For instance, peptide-amphiphiles [25,26], glutamide amphiphiles [27], glucolipids [28,29], phospholipids [30], cyclic peptides [31–35], and C3-symmetrical molecules [36] have been known to self-assemble into tubular architectures. Hollow spherical architectures self-assembled from π-conjugated molecules (porphyrins) [37], phospholipids [38,39], and surfactant [40,41] have also been demonstrated. Studies on hollow structures have mainly focused on their molecular design and characterization of morphology, while there has been little research dedicated to their chirality properties, especially the evolution of chiral emission, *i.e.*, circularly polarized luminescence, CPL.

Chirality is also the basic character of nature. Amino acid, protein and DNA all play important role in the biological system. The chirality transfer and tunable chirality are widely appeared in the living system. In this viewpoint, the modulation of chiral information, such as the chiroptical signals and helicity in the self-assemblies is meaningful to understand chiral phenomena in nature. Notably, the chiral inversion and amplification of chiroptical signals in the self-assemblies from small organic molecules [42–54] have attracted considerable attentions.

* Corresponding authors.
E-mail addresses: twang@ustb.edu.cn (T. Wang), zhangli@iccas.ac.cn (L. Zhang), liumh@iccas.ac.cn (M. Liu).

https://doi.org/10.1016/j.cclet.2023.109256
1001-8417/

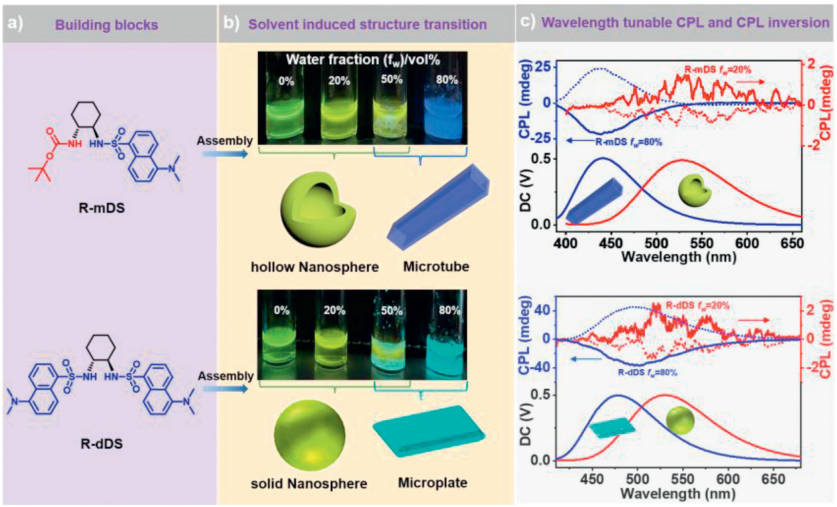

Scheme 1. (a) Molecular structures of asymmetric (R-mDS) and symmetrical (R-dDS) V-shaped molecules. (b) Solvent-tuned structure and emission transition of V-shaped molecules with increasing water fraction. (c) Wavelength tunable CPL and CPL inversion of V-shaped molecules at different water fraction.

Herein, we designed an asymmetric chiral V-shaped molecule (mDS) by attaching a dansyl moiety to a *trans*-*N*-Boc-1,2-cyclohexane diamine and found that it can self-assemble into hollow sphere and tubular structures through increase of water amount in H_2O/acetonitrile, as shown in Scheme 1. Meanwhile, the CPL signal of assemblies was demonstrated to be inversed and wavelength tunable. By contrast, we also synthesized a symmetric chiral molecule (dDS) by linked two dansyl groups to *trans*-1,2-cyclohexane diamine. Although the wavelength tunable and inversed CPL were investigated, no hollow structures were found in the self-assemblies of symmetric dansyl-linked cyclohexane diamine, where solid nanospheres transformed to solid microplates as water fraction increased.

It is well known that amide and sulfonamide bonds have different hydrogen bonding capabilities, which may lead to different self-assembly behaviors of the two V-shaped molecules, accompanied by different molecular arrangements. We first studied the self-assembly behavior of asymmetric V-shaped mDS molecules by adjusting the solvent ratio upon introducing antisolvent water into the acetonitrile solution. Taking R-mDS as an example, it could be well dissolved in acetonitrile upon heating and remained transparent after cooling to room temperature, and then antisolvent water was introduced to promote its self-assembly. Scanning electron microscopy (SEM) observation showed that R-mDS assembly exhibited the significantly punctured nanosphere structure where the water fraction (f_w, water volume fraction in the mixed solvent) was at 0%, and the nanosphere structure almost remained consistently unchanged as f_w increased to 40%. As the water fraction was increased to 50%–60%, microtubular structure with smooth surfaces appeared slowly, where the nanosphere and microtubular structure co-existed in the whole system. Then, when f_w was further increased to 70%–80%, the spherical structure disappeared, leaving only microtubular structures (Figs. 1a and b, and Fig. S9 in Supporting information). Fluorescence microscopy also demonstrated the emergence of nanospheres with holes and microtubes upon increasing f_w, in which nanospheres exhibited green fluorescence while microtubes showed blue fluorescence emission (Figs. 1c and d). Transmission electron microscopy (TEM) was further used to verify the hollow features for the obtained structures (Figs. 1e and f), revealing that the obvious contrast ratio between the interior and exterior of the two structures (Figs. 1e and f, and Figs. S10 and S11 in Supporting information). Dynamic light scattering (DLS) analysis revealed that the average diameter of about 230 nm at water fraction of 0–40% (Fig. S12 in Supporting information), which was constant with the results obtained from SEM images. Thus, we have successfully achieved a solvent-regulated structural transformation of R-mDS from hollow nanosphere to microtube, where water acted as an antisolvent to facilitate the approaching of V-shaped molecules and subsequently trigger self-assembled structure with ordered arrangements. Similarly, S-mDS showed the solvent-regulated structural transformation upon changing water fraction (Fig. S13 in Supporting information). For symmetric V-shaped molecule R-dDS, when f_w was low (0 and 20%), R-dDS assembly exhibited solid spherical structure. With the increase of water proportion ($f_w = 50\%$), the white precipitates gradually separated out, showing two kinds of structures of solid microplate and sphere coexisted in the system. When the water content was high enough ($f_w = 80\%$), only two-dimensional square plate structure formed (Fig. S14 in Supporting information). So, dDS could

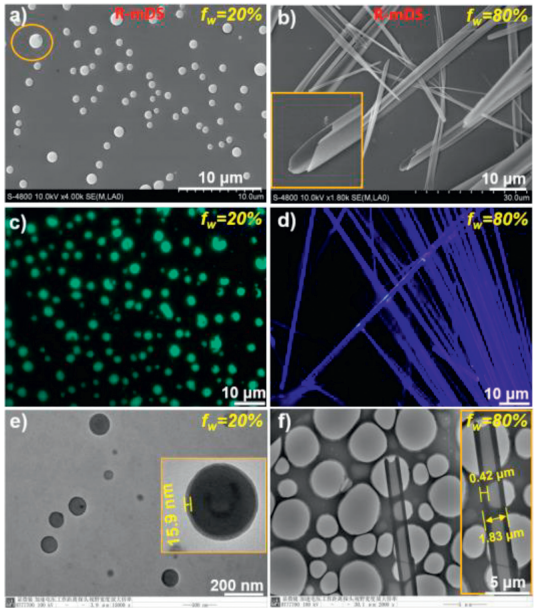

Fig. 1. SEM (a, b), fluorescence microscopy (c, d), and TEM images (e, f) of R-mDS assemblies at different water volume fractions ($f_w = 20\%$, $f_w = 80\%$, H_2O/acetonitrile). [R-mDS] = 8.63 mmol/L.

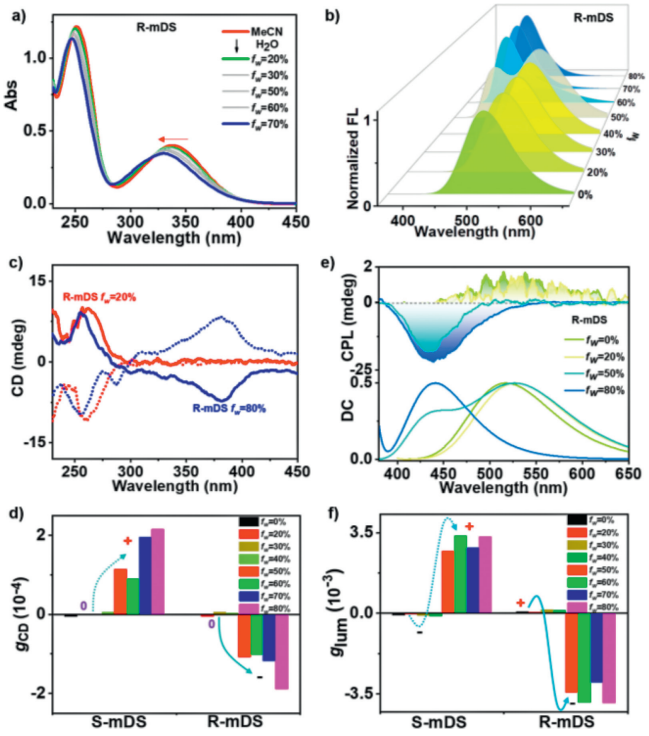

Fig. 2. UV–vis (a), CD spectra (c), asymmetric factor of CD signal at 379 nm (d). Fluorescence (Ex = 340 nm) (b), CPL (Ex = 340 nm) (e) spectra and asymmetric factor of CPL signal (f) for mDS assemblies at various f_w (H_2O/acetonitrile). [R-mDS] = [S-mDS] = 8.63 mmol/L.

also realize the structural transformation from solid nanospheres (green fluorescence) to solid microplates (cyan fluorescence) regulated by solvent ratio. The otherness in assembly structures of V-shaped mDS and dDS molecules may result from the differences in the hydrogen bonding between the sulfonamide and amide bonds, as well as the steric hindrance inherent in the molecules themselves.

UV–vis absorption spectroscopy was performed to analyze the formation of supramolecular structures upon adjusting the solvent ratio. R-mDS showed two absorption peaks at 251 and 337 nm, in which the absorption peak at 337 nm corresponds to the HOMO-LUMO transition obtained from time-dependent density functional theory (Fig. S15 and Table S1 in Supporting information) [55]. These absorption peak gradually hypsochromic shift with the increase of water content, suggesting that an H-like aggregation in the assemblies of R-mDS (Fig. 2a). Further, circular dichromic (CD) spectra were measured. Taking mDS as an example, R-mDS showed only one positive Cotton bond at 260 nm when f_w was below 50%, but another new and negative Cotton bond appeared at 379 nm when f_w was above 50% (Fig. 2c and Fig. S18 in Supporting information). The presence of the strong and negative CD signal at 379 nm indicated that the chirality transfer from chiral center to chromophore was enhanced upon increasing of water content during the structure transition from hollow spheres to microtubes (Fig. 2d). Moreover, the CD spectra of S-mDS were the mirror images of its enantiomer R-mDS at various water content, confirming that solvent regulated chiroptical signals amplification in the self-assembled mDS system.

It is known that dansyl could emit dual fluorescence bands, locally excited fluorescence (LE) and twisted intramolecular charge transfer fluorescence (TICT) due to its inherent molecular structure (flexibly twisted NMe2 group) [56,57], and the ratio of the two emission bands is sensitive to solvent polarity, viscosity, temperature, and pH, *etc*. In the self-assembly system of mDS, we achieved the transformation of LE and TICT emission by adjusting the water ratio, as shown in Fig. 2b. With the increase of water, the emission intensity at *ca*. 520 nm (TICT) for R-mDS assembly decreased, while the emission at 441 nm (LE) increased. The combination of its multicolor fluorescence emission and its chiral nature may give it unique CPL properties. As shown in Fig. 2e, R-mDS presented the very weak and positive signals in CPL investigation when f_w was less than 50%, and then turned into the relative strong negative CPL signals when f_w was larger than 50%. Then the results showed that the wavelength-tuned and inverted CPL signal could be regulated by the water ratio, accompanying with assemblies from hollow nanospheres to microtubes. Meanwhile, S-mDS had a similar wavelength-dependent CPL signal, as shown in Fig. 2f and Fig. S19 (Supporting information). The combination of CD and CPL spectra indicated that not only ground-state but also excited-state chirality of hollow nanospheres produced under lower f_w condition was much lower than that of hollow microtubes at higher f_w. As illustrated in Fig. S20 (Supporting information), the symmetric V-shaped molecule dDS presented comparable shifts in CD and CPL signals under water ratio modulation. Furthermore, the HOMO and LUMO energy levels were simulated through theoretical calculations (Fig. S17 in Supporting information). The results revealed that the HOMO-LUMO energy gap of R-dDS was smaller than that of R-mDS, suggesting that the electrons in R-dDS were more easily excited, causing a redshift in the excitation spectrum. This phenomenon was consistent with the experimental fluorescence spectra, manifesting as blue fluorescence for R-mDS and cyan fluorescence for R-dDS.

Similarly, the morphologies and chiroptical signals of the assemblies of mDS and dDS at mixed water and tetrahydrofuran showed a transformation from spherical structure to rod-like structure. Reversed and amplified chiral signals were observed at high water fraction (Figs. S21-S25 in Supporting information).

Furthermore, we monitored the dynamic transformation of self-assembled structure of R-mDS on standing time. Taken water amount of 50% as an example, the evolution of sphere to tubular structures was observed (Fig. 3). Fig. 3a shows the time-dependence fluorescence spectra. When water was just added to the acetonitrile solution (f_w = 50%), the system initially had a strong TICT fluorescence emission peak at 530 nm, and a new LE emission peak appeared at 441 nm upon prolonging time. The dynamic emission changes in the self-assembly process of R-mDS with the extension of time were shown in Fig. 3b. In the observation of fluorescence microscopy images (Figs. 3c-e), we could clearly capture the transition from the yellow-green fluorescent nanospheres to blue-fluorescent microtubes, accompanied by the coexistence of nanosphere and microtube in the middle process. Such evolution process from hollow nanospheres to microtubes could also be monitored by SEM (Figs. 3f-h).

To further understand the stacking patterns and self-assembly structures of mDS and dDS, single-crystal X-ray crystallography (Fig. 4) and powder X-ray diffraction (PXRD, Figs. S27 and S30 in Supporting information) techniques were applied. We successfully obtained single crystal of R-mDS and R-dDS. The crystal structures were analyzed by X-ray crystallography (Table S3 in Supporting information).

The single-crystal structure of the microtube self-assembled from R-mDS disclose an orthogonal chiral space group of $P2_12_12$ with four molecules in every single cell unit (Fig. S26a in Supporting information), which exhibit an unusual stereoscopic herringbone packing [58], each tilted relative to the ab-plane (Figs. S26c-d in Supporting information). Two neighboring molecules within a unit cell interact each other through the hydrogen bonds (2.40 Å, Fig. 4c, blue dashed lines) between the cyclohexane diamine hydrogen atom and *N*-dimethyl hydrogen atom. Adjacent unit cells in ab-plane are still stabilized upon bonding between cyclohexane

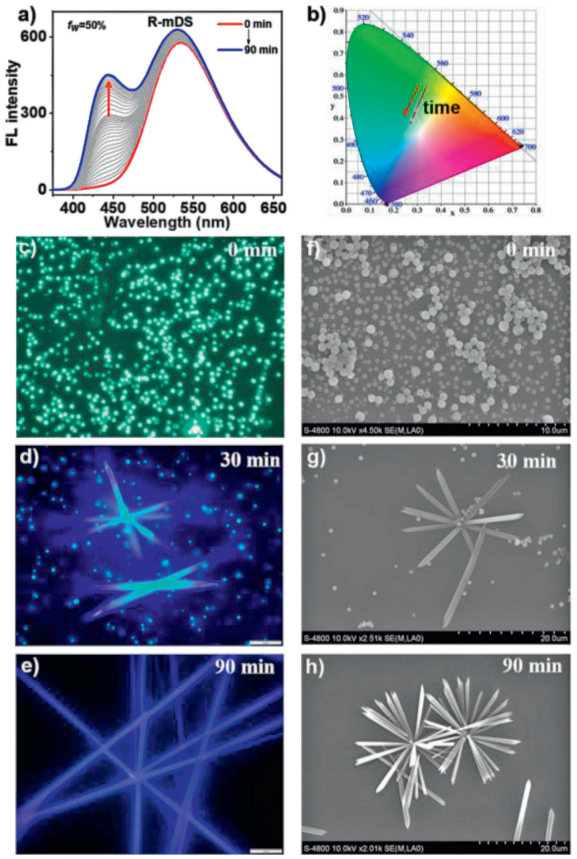

Fig. 3. Fluorescence spectra (Ex = 340 nm) (a) and CIE coordinates (b) of R-mDS assembly at different self-assembly time from 0 to 90 min (f_w = 50%, H_2O/acetonitrile). Fluorescence microscopy (c-e) and SEM (f-h) images of R-mDS (f_w = 50%, H_2O/acetonitrile) varied with time. Notes: (c, f) 0 min, (d, g) 30 min, and (e, h) 90 min. [R-mDS] = 8.63 mmol/L.

diamine hydrogen atom and *N*-dimethyl hydrogen atom (Fig. 4a). The R-mDS crystal exhibit a distinct non-coplanar zig-zag structure along c-axis, accompanying by parallel orientation across cell layers (5.19 Å) (Fig. 4b and Figs. S26e and f in Supporting information). Along c-axis, R-mDS molecules extend their structure by π-π interactions (3.46 Å, green solid lines in Fig. 4c) and two types of intermolecular hydrogen bonding interactions between the sulfonamides (2.10 Å, blue dashed lines) and the carboxyl amides (2.19 Å, red dashed lines), respectively.

In order to get insight of packing of R-mDS hollow sphere and microtube, XRD pattern of R-mDS sphere (f_w = 20%) and microtubes (f_w = 80%) were measured, which demonstrating more ordered XRD patterns of microtubes relative to that of spheres. Further, obvious peak at the D-space around 3.35–3.67 Å, which ascribed to π-π stacking, indicated that strong π-π stacking existed in microtube comparing with spheres (Fig. S27b in Supporting information).

R-dDS have an orthogonal chiral space group of $P2_12_12_1$ with four molecules in a unit cell (Fig. S28a in Supporting information). The R-dDS molecules exhibit the right-handed P-type spiral arrangement in the crystal [59–61], with a helical pitch of 10.12 Å (Fig. 4e). Within each R-dDS helix, every molecule undergoes a 180-degree rotation relative to its adjacent molecules along the 2_1 helical axis, leading to an antiparallel stacking arrangement, where the non-covalent intermolecular sulfonamide hydrogen bonds between sulfonamide hydrogen and sulfonamide oxygen periodically expand (Fig. 4f, green dashed lines, the distance of the sulfonamide hydrogen bonds is 2.20 and 2.16 Å, respectively). Evidently, the space-filling model of R-dDS molecule indicates that the sulfonamide hydrogen bonds also manifest a distinct P-helical hydrogen bond arrangement, which aligns with the P-helix organization of the R-dDS molecules (Fig. S28c in Supporting information). Moreover, these R-dDS helices (simplified as a spring model) organize into an array of springs in the bc-plane. This array obtained upon screwing (180°) and translating (13.35 Å) the adjacent column of spring (Figs. 4d and e, Figs. S28e and g). Two neighboring columns of helices are contacted by CH-π interactions (Fig. 4f, black dashes lines). The crystal structure of S-dDS molecules showed a similar

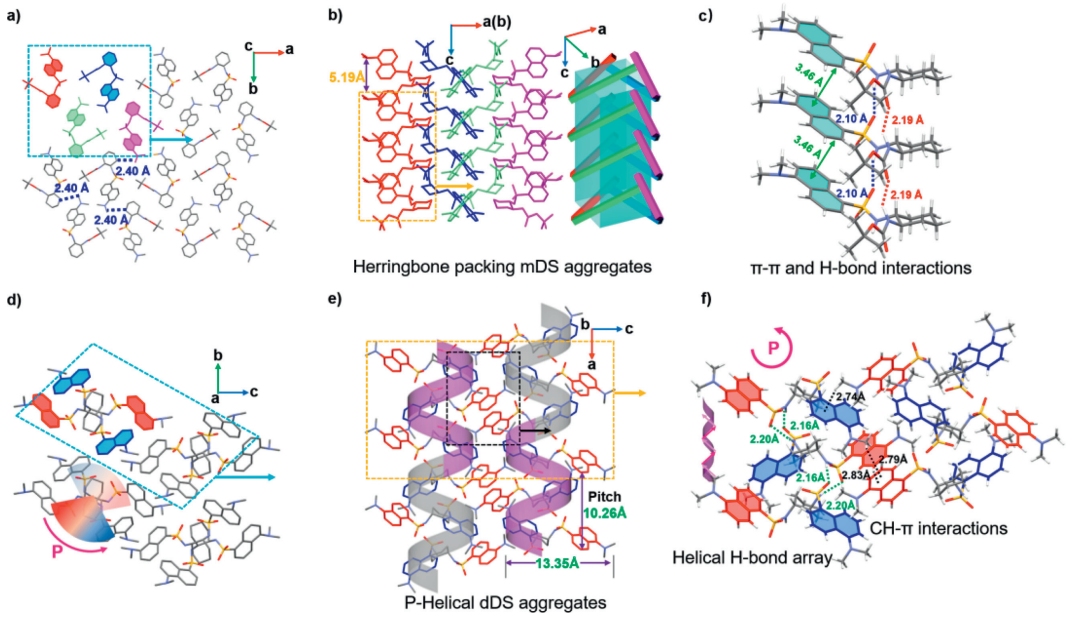

Fig. 4. Crystal structure analysis of R-mDS (a-c) and R-dDS crystal (d-f). (a) The top view of a single layer from the c-axis of the R-mDS crystal. (b) The side view of the R-mDS crystal shows the stereoscopic herringbone arrangement along c-axis. (c) The molecular packings and interlayer interactions along c-axis of the R-mDS crystal. (d) The top view of a single layer from the a-axis of the R-dDS crystal. (e) The side view of the R-dDS crystal shows the P-helical arrangement. (f) The molecular packings and interlayer interactions along a-axis of the R-dDS crystal.

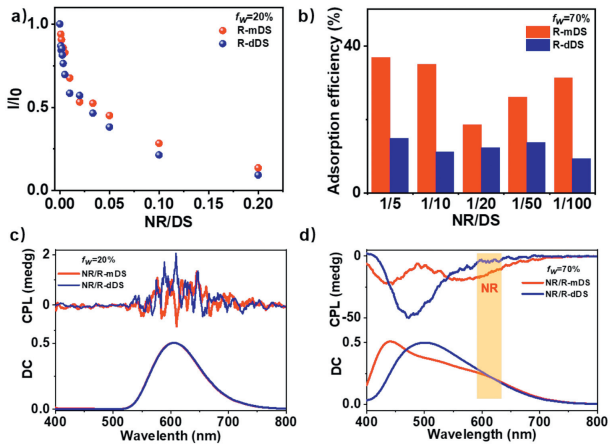

Fig. 5. (a) The relative emission intensities I/I_0 at 530 nm as different amount of NR to R-mDS (red spheres) and R-dDS (blue spheres), Ex = 340 nm. (b) The adsorption efficiency of NR for hollow microtubes formed by R-mDS and solid microplates formed by R-dDS at different NR/R-mDS and NR/R-dDS ratios. CPL spectra (Ex = 340 nm) of NR/R-mDS and NR/R-dDS (molar ratio 1/10) co-assemblies at f_w = 20% (c) and 70% (d) in H_2O/acetonitrile.

but opposite M-helical aggregates and M-helical H-bond array in contrast to R-dDS enantiomer (Figs. S28b, d, f, h and S29 in Supporting information).

Next, we investigated that the energy transfer and chirality transfer from DS assembly to achiral component, Nile Red (NR). Firstly, when f_w was 20%, we found the energy transfer from DS to NR of NR/R-mDS and NR/R-dDS co-assemblies due to considerable spectral overlap between the absorption band of NR and DS emission, which was characterized by the gradual decrease of TICT emission of DS with addition of NR (Figs. S31 and S32a in Supporting information). The hollow or solid nanospheres of DS showed similar quenching efficiency (Fig. 5a). The co-assemblies changed to blue or cyan emission when f_w increased, where the absorption of NR band was not overlap with the DS emission (Fig. S32a in Supporting information). Therefore, no effective energy transfer was found from DS to NR in NR/R-DS co-assemblies, as characterized by the retaining of DS emission with the addition of NR (Figs. S32b and c in Supporting information). The hollow tubular and solid platelike structures existed at high f_w and the adsorption capacity of these structures to NR were studied, which determined by absorption and fluorescence spectroscopy (Figs. S33 and S34 in Supporting information). It could be observed that under five different NR/R-m or dDS ratios, the adsorption efficiency of NR/R-mDS system were always higher than that of NR/R-dDS system, suggesting that hollow tubular structure had the higher wrapping capacity than solid platelike structure (Fig. 5b). Due to the intrinsic chirality of the two V-shaped molecules, the induced chirality of NR was also investigated (Figs. S35 and S36 in Supporting information). The induced CPL signals of NR in NR/R-mDS and NR/R-dDS co-assemblies were weak and positive when f_w was 20%, while the induced CPL of NR in NR/R-mDS and NR/R-dDS co-assemblies were negative when f_w was 70%, indicating chirality transfer from DS to Nile red (Figs. 5c and d). As a hydrophobic fluorescent dye, NR was loaded in the hydrophobic microenvironment of DS assembly. The π-π stacking between NR and dansyl moiety of DS was supposed to mainly contributed to the chirality transfer, which was similar with the results of NR in chiral assemblies of cyanostilbene or naphthalimide derivatives [62–64]. CPL signal of NR in NR/R-mDS co-assemblies was stronger than that in NR/R-dDS co-assemblies, which may attribute to the hollow tubular structure. Furthermore, inversion of CPL signal of NR in these two co-assemblies (Fig. S36 in Supporting information) was similar to the variation of the self-assemblies of R-m or dDS with the increase of water fraction although same enantiomeric V-shaped enantiomer R-DS was used, indicating that the CPL of NR was derived from the supramolecular chirality.

From the results of the morphology, optical and chiroptical properties of DS assemblies, the self-assembly of dansyl derivatives was proposed, as shown in Fig. 6. When the proportion of water were low (f_w < 50%), the *N,N*-dimethyl groups in both asymmetric mDS and symmetric V-shaped dDS molecules had the large twist angle relative to naphthalene plane, corresponding to the twisted intramolecular charge transfer (TICT) mode. In this case, the non-coplanar structure led to a larger steric hindrance of the V-shaped molecules in the process of self-assembly, and thus the spherical structures with the larger curvature were formed [65]. When the proportion of water were high ($f_w \geq$ 50%), the twisted angle of *N,N*-dimethyl groups with respect to naphthalene ring decreased. This coplanar (quinoid) structure had relatively small steric hindrance, leading to generate hollow microtubular structure (blue emission) for mDS with an unusual stereoscopic herringbone mode, packing through π-π stacking and the stronger hydrogen bond interactions. And the solid microplate structure (cyan emission) of dDS was formed with helical arrangement, which formed through the weaker sulfonamide hydrogen bond interaction. Comparing to the nanospheres, the CPL signal of both microtubes and

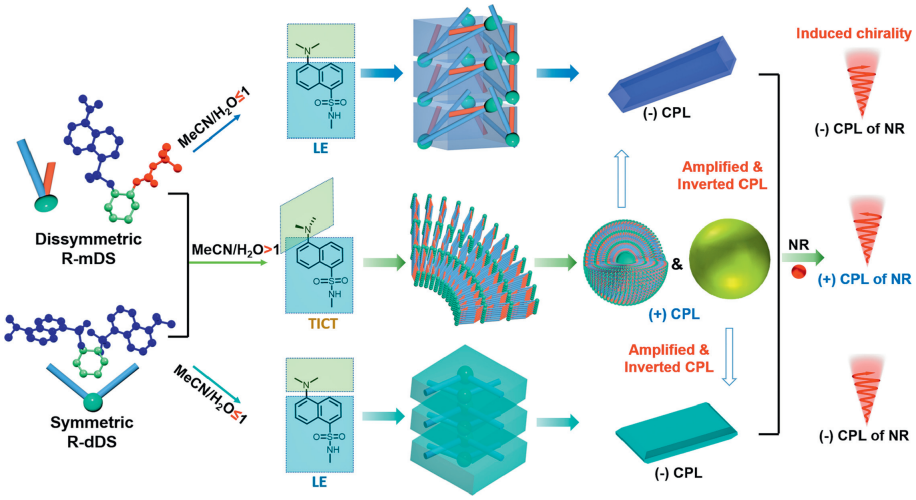

Fig. 6. The schematic illustration on self-assembly of R-mDS and R-dDS regulated by solvent and CPL of Nile red induced by supramolecular chirality in co-assemblies.

microplates due to the small steric hindrance were not only reversed but also amplified due to the closer packing of dansyl moiety. Further, induced CPL of Nile red also inverted in the co-assemblies with variation of water amount.

In conclusion, we synthesized asymmetric (mDS) and symmetric (dDS) chiral V-shaped molecules. Asymmetric mDS underwent the transition from hollow nanospheres to microtubes, as increasing f_w (water/acetonitrile). Symmetrical dDS occurred the similar structure transition from solid nanospheres to microplates. The increase of water also caused the emission change from green to blue or cyan, owing to the TICT to LE of dansyl moiety. The introduction of amide group in asymmetric mDS may increase the hydrogen bonding, leading to the emergence of tubular structures, which were constituted by stereoscopic herringbone microstructures that expanded along c-axis upon π-π stacking and hydrogen bond interactions. The tubular and platelike structures formed at higher f_w both showed the reversed and enhanced CPL compared to spherical structures. Further, induced CPL of achiral Nile red in the co-assemblies of DS/NR also inverted with increase of water amount, indicating that the induced CPL of NR was determined by the supramolecular chirality of DS assembly.

Declaration of competing interest

The authors declare that they have no known competing financial interests or personal relationships that could have appeared to influence the work reported in this paper.

Acknowledgments

We gratefully acknowledge financial support from the National Key R&D Program of China (No. 2021YFA1200301), the National Natural Science Foundation of China (Nos. 21890734, 92156018, and 21972150), and CAS Project for Young Scientists in Basic Research (No. YSBR-027).

Supplementary materials

Supplementary material associated with this article can be found, in the online version, at doi:10.1016/j.cclet.2023.109256.

References

[1] J. Wang, J. Shen, S. Zhang, et al., Adv. Opt. Mater. 10 (2022) 2200985.
[2] W. Wang, W. Zhao, T. Chen, et al., Adv. Funct. Mater. 31 (2021) 2010306.
[3] L. Peng, H. Peng, Y. Liu, et al., Sci. Adv. 7 (2021) eabi7403.
[4] V. Haridas, Acc. Chem. Res. 54 (2021) 1934–1949.
[5] D. Datta, S. Jana, O. Tiwari, Pept. Sci. 112 (2020) e24134.
[6] J. Guo, X. Yu, Z. Zhang, Y. Li, J. Colloid Interface Sci. 540 (2019) 134–141.
[7] L. Feng, J. Li, G. Day, X. Lv, H. Zhou, Chem 5 (2019) 1265–1274.
[8] X. Cai, J. Du, L. Zhang, et al., Chem. Commun. 55 (2019) 12176–12179.
[9] B. Gole, V. Stepanenko, S. Rager, et al., Angew. Chem. Int. Ed. 57 (2018) 846–850.
[10] S. Yang, Y. Yan, J. Huang, et al., Nat. Commun. 8 (2017) 15856.
[11] B. Qi, X. Guo, Y. Gao, et al., J. Am. Chem. Soc. 139 (2017) 12020–12026.
[12] X. Wang, J. Feng, Y. Bai, Q. Zhang, Y. Yin, Chem. Rev. 116 (2016) 10983–11060.
[13] S. Song, H. Zheng, H. Feng, Y. Zheng, Chem. Commun. 50 (2014) 15212–15215.
[14] Y. Jun, E. Lee, X. Wang, et al., Adv. Funct. Mater. 23 (2013) 3661–3667.
[15] J. Hu, Y. Guo, H. Liang, L. Wan, L. Jiang, J. Am. Chem. Soc. 127 (2005) 17090–17095.
[16] X. Wang, J. Han, C. Luo, et al., Small 17 (2021) 2101538.
[17] X. Wang, Q. Dong, H. Qiao, et al., Adv. Mater. 32 (2020) 2002853.
[18] X. Xu, Z. Zhang, X. Wang, Adv. Mater. 27 (2015) 5365–5371.
[19] J. Zhou, Z. Lin, M. Penna, et al., Nat. Commun. 11 (2020) 4804.
[20] M. Nambiar, M. Nepal, J. Chmielewski, ACS Biomater, Sci. Eng. 5 (2019) 5082–5087.
[21] L. Tian, J.Y. Li, F. Liang, et al., Appl. Catal. B: Environ. 225 (2018) 307–313.
[22] G. Maurya, D. Verma, A. Sinha, L. Brunsveld, V. Haridas, Angew. Chem. Int. Ed. 61 (2022) e202209806.
[23] L. Zhang, M. Deng, Y. Duan, et al., Nano Res. 15 (2022) 1079–1086.
[24] S. Kang, K. Kim, Y. Cho, et al., Angew. Chem. Int. Ed. 61 (2022) e202207310.
[25] M. Hendricks, K. Sato, L. Palmer, S. Stupp, Acc. Chem. Res. 50 (2017) 2440–2448.
[26] J. Kim, S. Kwon, S. Kim, et al., J. Am. Chem. Soc. 134 (2012) 20573–20576.
[27] X. Zhu, Y. Jiang, D. Yang, et al., Chem. Sci. 10 (2019) 3873–3880.
[28] M. Assali, J. Cid, I. Fernandez, N. Khiar, Chem. Mat. 25 (2013) 4250–4261.
[29] N. Kameta, K. Ishikawa, M. Masuda, M. Asakawa, T. Shimizu, Chem. Mat. 24 (2012) 209–214.
[30] X. Wang, H. Du, Z. Wang, W. Mu, X. Han, Adv. Mater. 33 (2021) 2002635.
[31] Q. Song, Z. Cheng, M. Kariuki, et al., Chem. Rev. 121 (2021) 13936–13995.
[32] F. Novelli, M. Vilela, A. Pazo, M. Amorin, J. Granja, Angew. Chem. Int. Ed. 60 (2021) 18838–18844.
[33] J. Yang, J. Song, Q. Song, et al., Angew. Chem. Int. Ed. 59 (2020) 8860–8863.
[34] A. Pizzi, H. Ozores, M. Calvelo, et al., Angew. Chem. Int. Ed. 58 (2019) 14472–14476.
[35] R. Chapman, M. Danial, M. Koh, K. Jolliffe, S. Perrier, Chem. Soc. Rev. 41 (2012) 6023–6041.
[36] N. Matsumoto, R. Lafleur, X. Lou, et al., J. Am. Chem. Soc. 140 (2018) 13308–13316.
[37] Y. Liu, H. Wang, S. Li, et al., Nat. Commun. 11 (2020) 1724.
[38] N. Kameta, W.X. Ding, H. Uzawa, Chem. Mat. 34 (2022) 9425–9436.
[39] M. Tsuei, M. Shivrayan, Y. Kim, S. Thayumanavan, N. Abbott, J. Am. Chem. Soc. 142 (2020) 6139–6148.
[40] K. Liu, X. Qiao, C. Huang, et al., Angew. Chem. Int. Ed. 60 (2021) 14365–14369.
[41] M. Hanafusa, Y. Tsuchida, K. Matsumoto, K. Kondo, M. Yoshizawa, Nat. Commun. 11 (2020) 6061.
[42] J. Zhang, Q. Li, Y. Wang, et al., Adv. Mater. Interfaces 9 (2022) 2102089.
[43] R. Rodriguez, C. Naranjo, A. Kumar, et al., J. Am. Chem. Soc. 144 (2022) 7709–7719.
[44] S. Okuda, N. Ousaka, T. Iwata, et al., J. Am. Chem. Soc. 144 (2022) 2775–2792.
[45] Q. Xia, L. Meng, T. He, et al., ACS Nano 15 (2021) 4956–4966.
[46] M. Sleczkowski, M. Mabesoone, P. Sleczkowski, A. Palmans, E. Meijer, Nat. Chem. 13 (2021) 200–207.
[47] F. Wang, F. Gan, C. Shen, H. Qiu, J. Am. Chem. Soc. 142 (2020) 16167–16172.
[48] N. Kameta, T. Shimizu, Nanoscale 12 (2020) 2999–3006.
[49] J. Zhang, Q. Liu, W. Wu, et al., ACS Nano 13 (2019) 3618–3628.
[50] S. Lee, K. Kim, S. Jung, et al., Angew. Chem. Int. Ed. 58 (2019) 18878–18882.
[51] C. Kulkarni, P. Korevaar, K. Bejagam, et al., J. Am. Chem. Soc. 139 (2017) 13867–13875.
[52] X. Wu, M. Liu, C. Zheng, et al., Chin. Chem. Lett. 34 (2023) 107590.
[53] C. Wang, T. Jiang, X. Ma, Chin. Chem. Lett. 31 (2020) 2921–2924.
[54] Y. Xia, A. Hao, P. Xing, Chin. Chem. Lett. 34 (2023) 107955.
[55] T. Lu, F. Chen, J. Comput. Chem. 33 (2012) 580–592.
[56] Z. Grabowski, K. Rotkiewicz, W. Rettig, Chem. Rev. 103 (2003) 3899–4031.
[57] F. Vogtle, S. Gestermann, C. Kauffmann, et al., J. Am. Chem. Soc. 121 (1999) 12161–12166.
[58] S. Wang, Y. Liu, X. Yu, et al., Angew. Chem. Int. Ed. 60 (2021) 3979–3983.
[59] Y. Wang, D. Niu, G. Ouyang, M. Liu, Nat. Commun. 13 (2022) 1710.
[60] Z. Liu, J. Ren, P. Li, et al., Angew. Chem. Int. Ed. (2022) e202214211.
[61] Y. Gao, J. Zhao, Z. Huang, et al., Angew. Chem. Int. Ed. 61 (2022) e202201793.
[62] Z. Cao, A. Hao, P. Xing, Nanoscale 13 (2021) 700–707.
[63] Z. Cao, B. Wang, F. Zhu, A. Hao, P. Xing, ACS Appl. Mater. Interfaces 12 (2020) 34470–34478.
[64] Q. Cheng, A. Hao, P. Xing, Nat. Commun. 12 (2021) 6320.
[65] K. Liu, L. Meng, S. Mo, et al., J. Mater. Chem. C 1 (2013) 1753–1762.